This is a repository copy of *Film thickness measurements in a running hydrostatic unit using ultrasound*.

White Rose Research Online URL for this paper:
https://eprints.whiterose.ac.uk/131129/

Version: Accepted Version

eprints@whiterose.ac.uk
https://eprints.whiterose.ac.uk/

Film thickness measurements in a running hydrostatic unit using ultrasound

L. Leonhard[1], S. Marsch[1]*, P. Harper[2], R.S. Dwyer-Joyce[3]
[1]*Danfoss Power Solutions GmbH & Co. OHG, Neumünster, Germany*
[2]*Tribosonics Ltd, Sheffield, United Kingdom*
[3]*University of Sheffield, Department of Mechanical Engineering, Sheffield, United Kingdom*

Abstract

The present paper describes the measurement of the oil film thickness in the range of a few micrometers in an operating hydrostatic unit using ultrasound. The investigated tribological system consists of a rotating steel cylinder block and a stationary bi-metal valve plate under static and hydrodynamic lubrication. The film thickness has been recorded in a wide range of operating conditions, pressure between 100 to 300 bar and rotational speed between 500 and 3000 rpm, to support a deeper understanding of the system. Temperature sensors were implemented next to the ultrasound sensors to compensate the ultrasound signal amplitude and phase change due to temperature dependent acoustic impedances. To confirm the results, especially the presence of deliberate zero-film conditions, wear profiles of the running surface were taken.

The ultrasound technique also allows the real-time observation of film thickness oscillations with shaft and piston frequency. Steady-state measurements confirm the system behavior observed in transient operation and zero-film conditions with respect to hardware configuration were detected. The findings will be utilized to support current product development activities and to validate and improve simulation models used for film thickness predictions.

Keywords: Ultrasound, hydrostatic swash plate unit, oil film thickness, cylinder block, valve plate.

*Corresponding author: Contact by phone +49 4321 871 901 or by email smarsch@danfoss.com.

1. INTRODUCTION

In hydrostatic components the oil film between the loaded parts under relative motion determines the volumetric flow as well as mechanical losses. During normal unit operation, the hydrodynamic oil film balances the loading forces and provides bearing function. When hydrodynamic forces cannot balance the loading forces, zero-film conditions lead to metallic contact and subsequent wear. Thus, sufficient hydrodynamic lubrication through the oil film is a key factor for the lifetime of the hydrostatic components. In the last decade, ultrasound has become an important measurement technique in detecting films in the range of a few micrometers in tribological systems such as bearings or seals [1]. The present paper describes the first-time usage of this technique in an operating hydrostatic unit for the measurement of the oil film thickness between two main parts, namely cylinder block and valve plate. By measuring the proportion of ultrasound waves reflected at the oil film interfaces,

the ultrasound method allows a less indirect access to the oil film thickness compared to past methods that relied on information such as the valve plate temperature field or the relative position of cylinder block with respect to the valve plate. A good overview of past investigations associated with this interface is given in [2].

2. BACKGROUND

2.1. Tribological system

Hydrostatic pumps and motors convert mechanical energy into hydraulic energy and vice versa. In a swash plate type pump, see schematic in Fig. 1, the cylinder block is driven by the drive shaft. The pistons located in the cylinder bores perform a translational movement when sliding with their slippers on the inclined swash plate. By changing the displacement angle β, the unit displacement volume can be adjusted. During half of one revolution, the pistons move from inner dead point (IPD) to outer dead point (ODP),
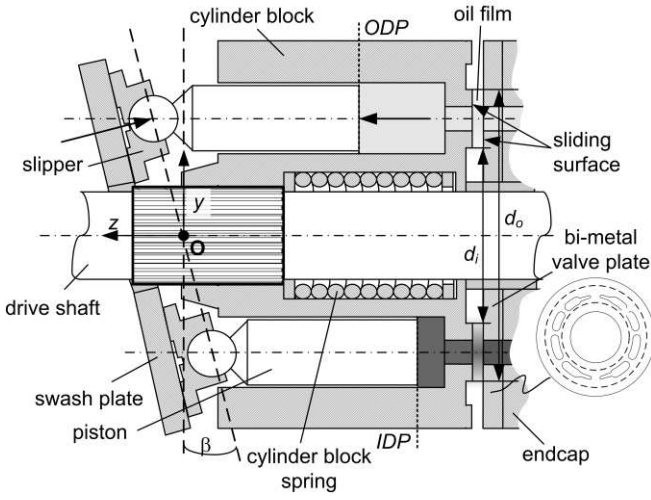
Figure 1: Principle of a swash plate type hydrostatic pump

while fluid is drawn into the displacement chamber from the low pressure port. Moving in the opposite direction from ODP to IDP during the second half of the revolution, the pistons push out the fluid from the displacement chamber into the high pressure port. The unit used during this investigation has an odd number of pistons ($k = 9$), resulting in a periodic change of either four or five cylinder bores connected to high pressure. The cylinder block is hydrostatically balanced by the pressure field across its running surface of the valve plate. In [3], balance ratios are given between 92 % up to 98 % relative to the smallest loading force. The ratio can be adjusted by changing the inner d_i and outer diameter d_o of the running surface (cf. Fig. 1). The remaining portion of the loading forces is balanced hydrodynamically. For sufficient hydrodynamic lubrication the cylinder block has to incline slightly relative to the valve plate. This degree of freedom is provided by the spherical spline geometry of the drive shaft. Two hardware parameters known to strongly influence the hydrodynamic performance were changed in this study, intending zero-film conditions for validation of the measurement results. One parameter is the spring force F_s pushing the block towards the valve plate. The spring force is necessary to prevent cylinder block lift at high-speed, low-pressure operating conditions. The second parameter is the bearing location of the cylinder block on the drive shaft usually determined by the intersection point between the shaft axis and the plane through the piston sphere centers (point O). Thus, it is located half way between the sphere centers of the pistons in IDP and ODP. As a consequence, the forces

transmitted from the individual pistons together with the reaction force from the shaft have only a low resulting moment M_x on the cylinder block. The dominant pressure force $F_{P,i}$ acting on every individual piston is balanced by a reaction force perpendicular to the swash plate $F_{SP,i}$, see Fig. 2. The remaining forces acting on the i-th piston represent a marginal portion of the total force. In consequence, these forces, i.e. inertia and frictional forces, are neglected. The y-component of the reaction force $F_{SP,i}$ acting perpendicular to the i-th piston axis depends on the displacement angle β.
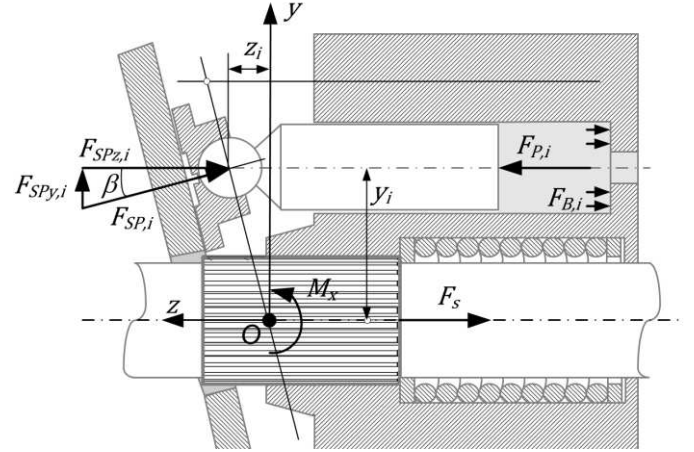

Figure 2: Dominant forces acting on the piston and block

$F_{SPy,i}$ is transmitted to the cylinder block through the piston guide, generating a pressure field between piston and block. The force $F_{SPy,i}$ together with the lever arm z_i creates a tilting moment about the bearing location on the cylinder block. The pressure acting on the i-th cylinder bore walls creates the force $F_{B,i}$ which results together with the lever arm y_i in a tilting moment. The resulting moment created by these forces can then be expressed with Eq. 1. A comprehensive overview of the acting forces is given in [3].

$$M_x = \sum_{i=1}^{k} y_i \cdot F_{B,i} + \sum_{i=1}^{k} z_i \cdot F_{SPy,i} \qquad \text{(Eq 1)}$$

Moving the bearing location (point O) in the direction of the valve plate – realized by modifying the spherical shaft spline – changes the corresponding lever arm z_i and leads to a significantly higher moment M_x on the cylinder block. This additional moment has to be supported by the oil film between cylinder block and valve plate. When the oil film cannot carry the total load, the bronze layer of the bi-metal valve plate

together with the steel block provides reasonable tribological performance in the mixed lubrication regime.

2.2. Ultrasound

When an ultrasound wave strikes an interface of two materials, the wave splits up in a transmitted and a reflected portion. Energy will be extracted from the incident pulse when a portion is transmitted into the medium which results in an amplitude and phase change of the reflected wave. As described in [1] the amount of reflection is dependent upon the acoustic impedance mismatch between those two materials z_1 and z_2; also known as the refection coefficient R described with Eq. 2.

$$R = \frac{z_1 - z_2}{z_1 + z_2} \qquad (Eq\ 2)$$

A fluid film between two surrounding parts can be modeled as a three-layer system [1]. Reflection and transmission take place at all interfaces of the three-layer system as shown in Fig. 3.
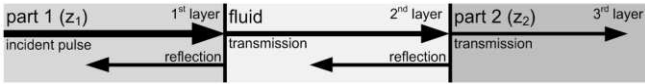

Figure 3: Three layer system with reflection and transmission at interfaces

When the wavelength of the ultrasound wave is large compared to the fluid film thickness ($\lambda \gg h$), the fluid film acts as unique reflector. Fluid mass and damping have negligible effect, while the reflection is dominated by the stiffness of the imbedded fluid layer. The reflection coefficient can then be obtained from Eq. 3, where z_1 and z_2 are the acoustic impedances of the surrounding materials, K is the fluid layer stiffness, and ω the angular frequency.

$$R = \frac{z_1 - z_2 + i\omega\left(\frac{z_1 z_2}{K}\right)}{z_1 + z_2 + i\omega\left(\frac{z_1 z_2}{K}\right)} = |R|\, e^{i\omega \Phi_R} \qquad (Eq\ 3)$$

When the wave front is large compared to the fluid film thickness h, the fluid is constrained to deform across its thickness only, i.e. the fluid area remains constant and the stiffness K of the liquid film can be obtained from the fluid bulk modulus B.

$$K = B/h \qquad (Eq\ 4)$$

Combining Eq. 3 and Eq. 4 and rearranging leads to Eq. 5 and Eq. 6, giving the relationship between film thickness and reflection coefficient amplitude $|R|$ on the one hand and film thickness and reflection coefficient phase Φ_R on the other hand.

$$h = \frac{B}{\omega z_1 z_2} \sqrt{\frac{|R|^2 (z_1 + z_2)^2 - (z_1 - z_2)^2}{1 - |R|^2}} \qquad (Eq\ 5)$$

$$h = \frac{B \cdot z_2 \pm B\sqrt{(tan^2\Phi_R + 1)z_2{}^2 - tan^2\Phi_R \cdot z_2{}^2}}{\omega z_1 z_2 \cdot tan\Phi_R} \qquad (Eq\ 6)$$

The method to obtain $|R|$ and Φ_R from the recorded pulses is described in the following section. For further information on film thickness measurements using ultrasound the reader should refer to [1].

2.3. General signal processing

In order to obtain $|R|$ and Φ_R, the in-situ pulses during operation are compared to a reference pulse. The reflection coefficient of a metal to air interface is known to be close to unity.
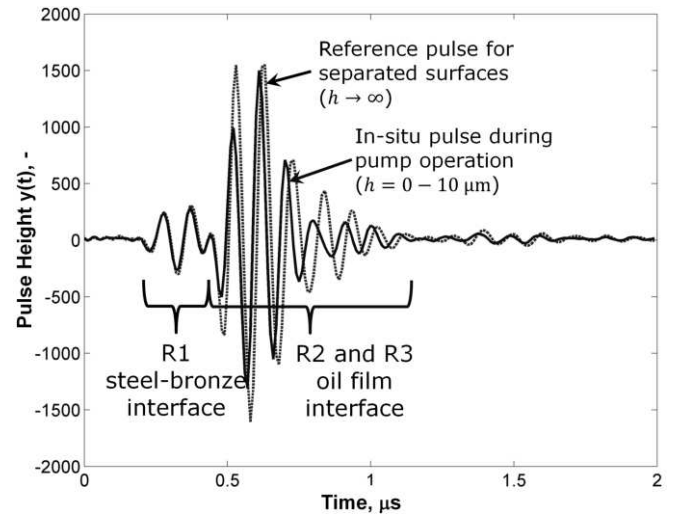

Figure 4: Reference and in-situ pulse versus time

Therefore, the reference pulse is taken prior to the actual measurements from a clean valve plate without counterface. In Fig. 4 an exemplary reference pulse and in-situ pulse are depicted. Because a bi-metal valve plate with a bronze layer is used, a first weak reflection R1 occurs at the steel-bronze interface. As explained before, the oil film acts as a unique reflector

3

and the two reflections at the two oil interfaces can be seen as one strong reflection R2 plus R3. It is obvious that the oil film leads to lower amplitude of the pulse as well as a phase difference compared to the reference pulse. A fast Fourier transform is performed on both pulses resulting in amplitude and phase spectra of the reference and in-situ pulses (see Fig. 5). Taking advantage of the fact that the reflection coefficient of the reference pulse is known to be unity, the reflection coefficient of the oil film can be obtained from the ratio of the amplitude spectrum of the in-situ and the reference pulse, see Eq. 7.

$$|R| = \frac{A(f)}{A_{ref}(f)} \cdot \underbrace{|R_{ref}|}_{\approx 1} \qquad \text{(Eq 7)}$$

The phase difference is obtained by subtraction of the phase spectrum of the in-situ pulse from the phase spectrum of the reference pulse, see Eq. 8.

$$\Phi_R = \Phi - \Phi_{ref} \qquad \text{(Eq 8)}$$

The results should only be considered within the range of the usable bandwidth, indicated by dashed lines in Fig. 5, of the ultrasound transducers due to low signal-to-noise-ratio outside this range.
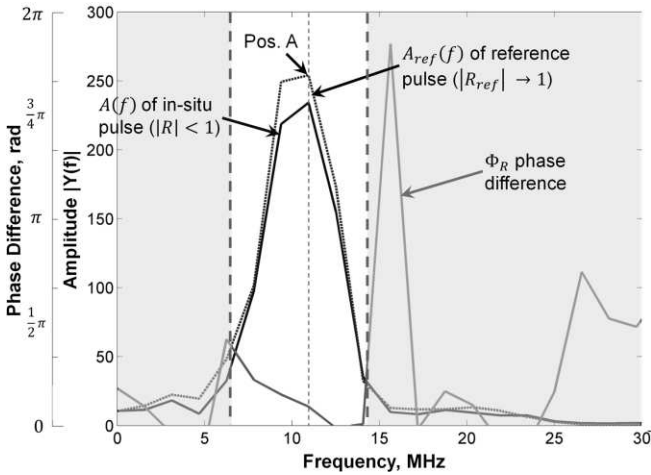
Figure 5: Phase difference and amplitude spectrum of reference and in-situ pulse

In order to compensate for temperature dependent acoustic properties of the system, the amplitude and phase profiles of the reference pulse have been recorded over temperature and implemented into the signal processing for each individual sensor. In Fig. 6, exemplary profiles are shown for the frequency where the amplitude spectrum is maximum (Pos. A in Fig. 5). The reference signal shifts constantly while the amplitude remains almost unaffected. Finally, the film thickness can be obtained from Eq. 5 and Eq. 6.
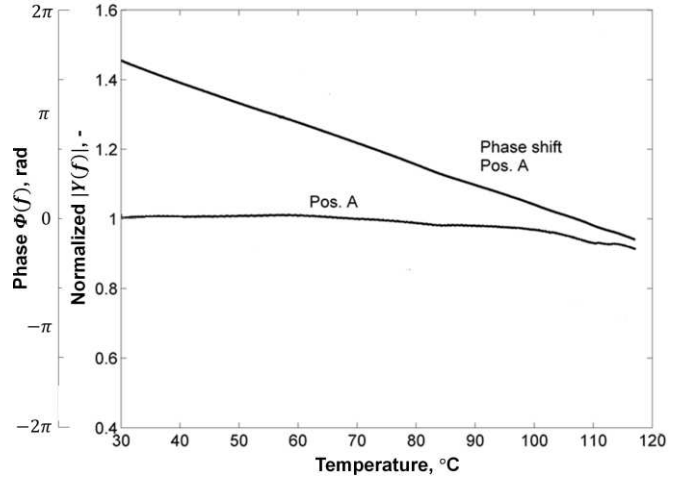
Figure 6: Temperature dependent amplitude and phase change of reference pulse

2.4. Analysis of errors

First, the film thickness determination from Eq. 5 and Eq. 6 is governed by the recorded amplitude and phase of the both in-situ and reference pulse. The amplitude uncertainties of the in-situ and reference pulse are considered to be the same. Same applies for the phase uncertainty. These uncertainties were determined recording a series of pulses with separate surfaces at a constant temperature. A normal distribution was adopted and the uncertainty was defined as 2σ around the mean value. The results are summarized in Eq. 9.

$$\Delta A = \pm 10 \text{ digits} \qquad \Delta \Phi = \pm 0.02 \text{ rad} \qquad \text{(Eq 9)}$$

Secondly, the film thickness is influenced by the local pressure and temperature determining the local bulk modulus. A polynomial function based on measurement data of the used mineral oil was used to calculate the bulk modulus. The bulk modulus increases with rising pressure and decreases with rising temperature. To take into account the difference in local oil film temperature and the local temperature measured on the back side of the valve plate (see Fig. 8), the uncertainty is estimated to

$$\Delta T_{local} = \pm 20 \,°C. \qquad \text{(Eq 10)}$$

4

The local film pressure is estimated by solving for the pressure field assuming fluid flow between parallel sliding surfaces. The uncertainty of the pressure estimation is defined as a proportion of the calculated local film pressure, see Eq. 11, including the uncertainty of the corresponding ultrasound sensor position.

$$\Delta p_{local} = \pm \, p_{local} \cdot 20\,\% \qquad \text{(Eq 11)}$$

Thirdly, the bulk modulus is influenced by the amount of free air in the oil. Air inclusions in low pressure cause a significant reduction of the bulk modulus, while for high pressure the influence is insignificant. Consequently, air inclusions in low pressure result in a decrease of the film thickness. However, a sufficient high film thickness is indicated in the low pressure region by simulation results and wear patterns of used valve plates. In consequence, free air is considered as uncritical and not relevant for this study. The oil bulk modulus function is substituted into Eq. 5 and Eq. 6 before calculating the film thickness uncertainties by the Gaussian error propagation law.
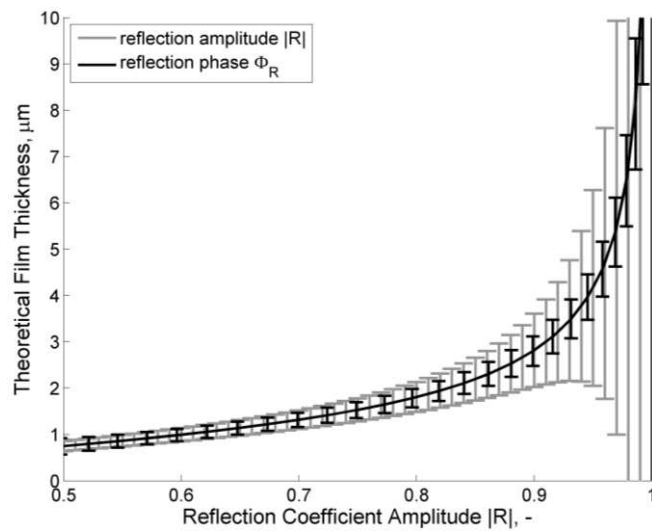

Figure 7: *Theoretical film thickness versus reflection coefficient amplitude with estimated error at 50 °C and 100 bar*

The film thickness uncertainty as function of reflection coefficient amplitude is illustrated in Fig. 7 for one parameter constellation with the described errors. The relationship of reflection coefficient amplitude and phase is determined by combining Eq. 5 and Eq. 6. As the reflection coefficient amplitude approaches unity, the calculated theoretical film thickness tends to

infinity. In consequence, the reflection-coefficient operating range is limited to 0.99. It is clear by the equations that the estimated error in this region derived from Eq. 5 is higher as derived with Eq. 6. To take advantage of the different error situation both equations have been adopted in the scope of this study. Additional information related to the uncertainty and calibration of the ultrasound film thickness measurement can be found in [4].

3. TEST SETUP AND CONDITIONS

Fig. 8 shows the tribological system with the sensors that transmit and capture the pulses. In total eight sensors are located on the back side of the valve plate distributed with respect to the running surface. The pulser-receiver-device is controlled by a *LabView* program.
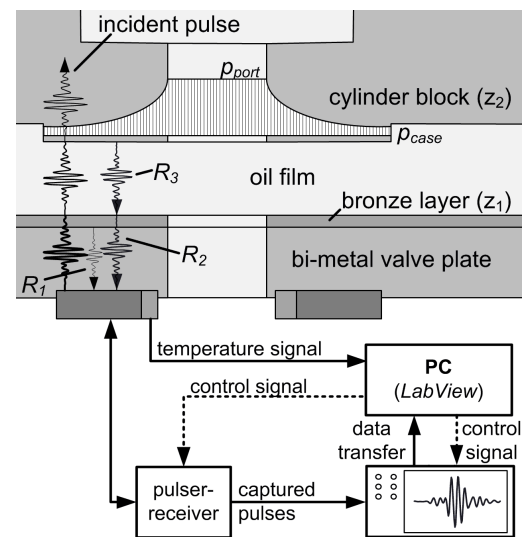

Figure 8: *Tribological system with the data acquisition and control system (film thickness largely exaggerated)*

A small portion (R1) of the incident pulse is reflected at the steel-bronze interface of the bi-metal valve plate. The transmitted portion reflects again (R2) at the first oil interface – bronze to oil. After passing the oil film the pulse is again (R3) reflected by the rotating cylinder block at the second oil interface – oil to steel. Reflection R3 then combines with R2 to a unique pulse. To compensate the ultrasound signal amplitude and phase change with temperature, temperature sensors are located next to the ultrasound sensors. The film thickness was recorded in a wide range of steady-state operating conditions, pressure between

5

100 to 300 bar and rotational speed between 500 and 3000 rpm, to support a deeper understanding of the system. Additionally, speed ramps were performed while holding pressure constant. The oil temperature was held constant at 50 °C regarding the high pressure port.

By changing two hardware parameters, three different hardware configurations were analyzed, listed in Table 1. The bearing position of cylinder block on shaft was shifted from point O (in O) out of this location towards valve plate (out of O). Secondly, the spring force on the cylinder block was varied between reduced and increased spring force. A single valve plate was used during testing. To monitor the wear progress, several wear profiles of the running surface were taken in radial direction after each test series for the individual hardware configuration (one profile location depicted in Fig. 10). Mineral oil based hydraulic fluid HM46 according to ISO 6743-4 was used during testing.

Table 1: Investigated hardware configurations

	ConFig. 1:	ConFig. 2:	ConFig. 3:
Bearing	in O	out of O	in O
Spring	reduced	reduced	increased

The short test time has no impact on oil degradation resulting in poor data quality. However, the effect of oil degradation could be part of future investigations regarding impact on film thickness.

4. RESULTS

4.1. General film thickness results

The film thickness was calculated with help of Eq. 5 and Eq. 6, implementing the bulk modulus dependent on an estimated local film pressure and temperature. The estimation is based on a logarithmic pressure profile exemplarily shown in Fig. 8, and the measured temperatures on the back side of the valve plate. The pressure profile was calculated assuming parallel sliding surfaces. Fig. 9 depicts the film thickness versus time. The left and the right side of the diagram were calculated based on the reflection coefficient amplitude (Eq. 5) and phase (Eq. 6), respectively.
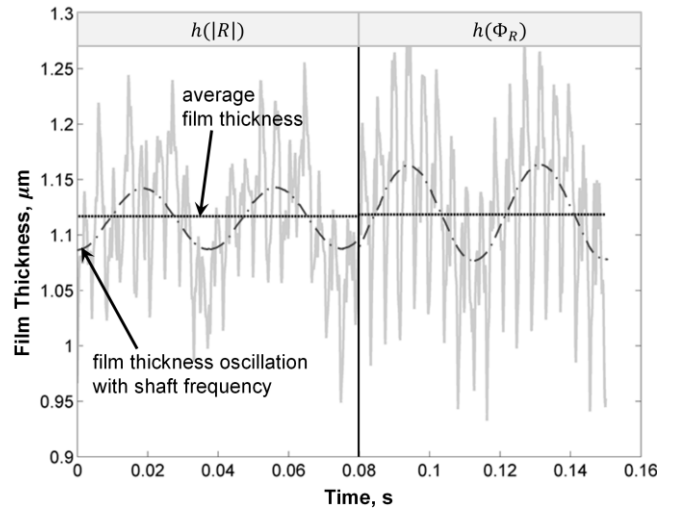

Figure 9: Example of recorded film thickness versus time (using a low pass filter with corner frequency of f_9)

The deviation of these two methods is in the range of measurement uncertainty. The film thickness oscillates with shaft frequency superimposed with its higher orders f_9 and f_{18}. These can be calculated with the number of pistons k and shaft speed n, see Eq. 12. The oscillations reflect the fact that the changing load forces of the system have to be compensated by the hydrodynamic lubrication film.

$$f_9 = k \cdot n \text{ and } f_{18} = 2 \cdot k \cdot n \qquad \text{(Eq 12)}$$

The average film thickness of all eight individual sensor locations are used to linearly interpolate the film thickness over the valve plate in radial and circumferential direction for better visualization (see Fig. 10).
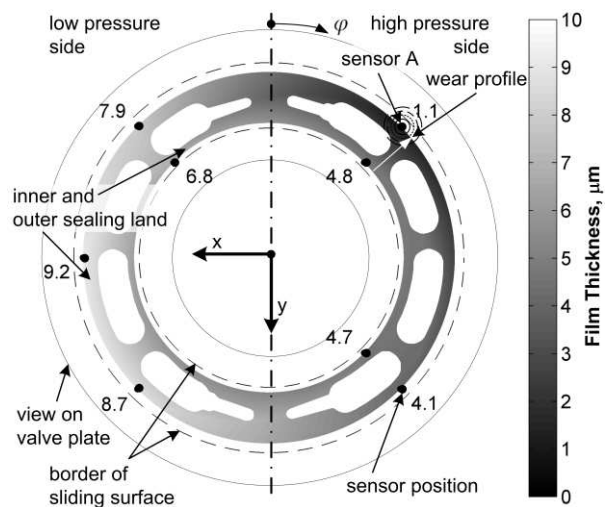

Figure 10: Example of recorded film thickness between cylinder block and valve plate

However, the film thickness can be non-linear due to elastic deformation, especially on the high pressure side. Therefore, the color does not represent the real film thickness between the sensor locations, but is a good visual indicator of thin-film locations. The measurement equipment options were deliberately selected to primarily detect thin films. These options together with a limitation of the reflection coefficient amplitude to 0.99 (see pole in Eq. 5) determine a maximum measurable film thickness of 10 μm in this study, see scale in Fig. 10. By adjusting the measurement equipment options, a more realistic representation of the film thickness can be generated also for the thick-film locations. In this study the cylinder block rotates in clockwise direction, indicated by φ, while the right side and left side are at high pressure and low pressure, respectively.
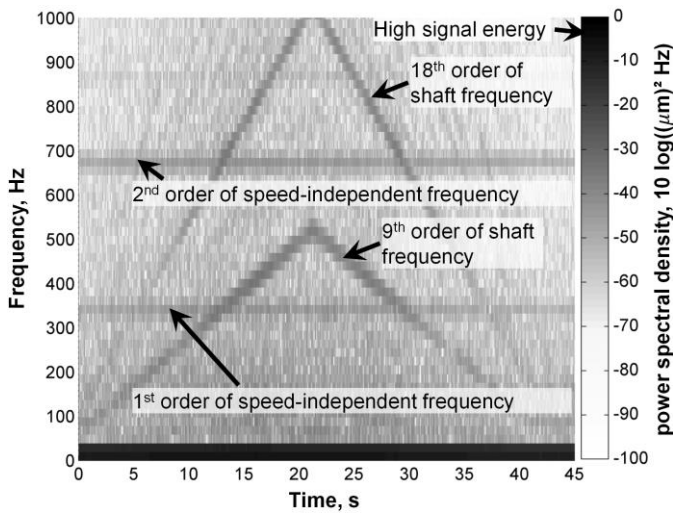

Figure 11: Exemplary film thickness spectrogram of highlighted sensor A with configuration 1 at 100 bar

Speed ramp operating conditions are presented with the help of spectrograms showing the power spectral density as depicted in Fig. 11. According to Eq. 12, the spectrograms reflect the in- and decrease in speed n by a linear increase of the higher order shaft frequencies f_9 and f_{18}. Additionally, the first and second order of a speed-independent frequency of the system can be seen in the spectrogram. Identifying the source of this frequency was not in the scope of this study.

4.2. Results regarding different hardware configurations

Table 2 contains the surface plots for all three tested hardware configurations at 100 bar and different speeds, while Table 3 contains the wear profiles taken after every hardware configuration change. No film thickness smaller than 1.9 μm can be observed in the surface plots for hardware configuration 1. The thinnest film at 500 rpm in the inner ring can be regarded as uncritical, supported by the wear profile.

Table 2: Average film thickness for hardware configurations 1 to 3 at 100 bar *and three different rotational speeds*

The film thickness plots for hardware configuration 2 with shifted bearing location O reflects the significantly increased moment on the cylinder block M_x. The resulting moment leads to a thin film (≤ 1 μm) on the high pressure valve plate side at the outer diameter of the running surface for all speeds. In contrast, the surface plots indicate a sufficiently thick film at the inner diameter region versus speed. With higher shaft speeds, hardware configuration 2 starts to behave instable. This is observable as broadband film thickness oscillation in the spectral density depicted in Fig. 12, starting at approximately 20 s (3200 rpm) for 100 bar.
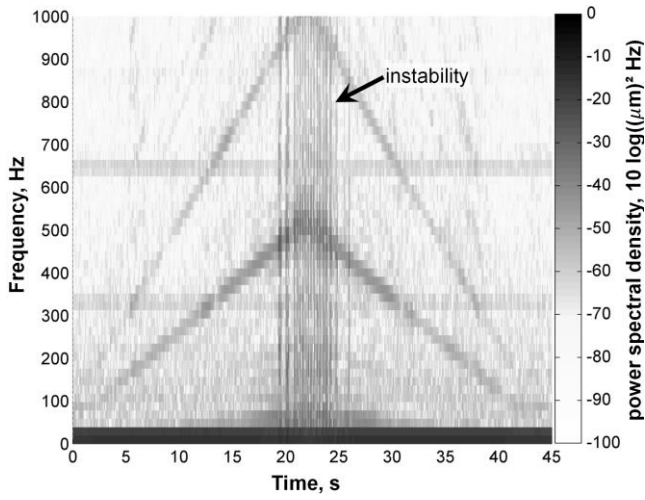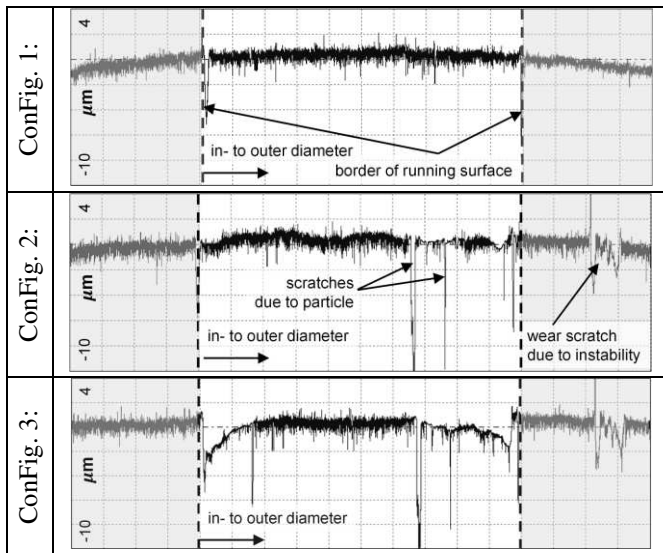
Figure 12: Film thickness spectrogram of highlighted sensor A with configuration 2 at 100 bar

Table 3: Wear profile after tests with configuration 1 to 3, measured at location of white arrow in Fig. 7

Comparing the surface plots of hardware configuration 1 and 2 with the surface plots of hardware configuration 3, reveals a significant influence of the increased spring force. A thin film is recorded at the inner diameter region, which stays constantly thin on both pressure sides versus speed. Moving the bearing location back to O prevented the system instability observed for hardware configuration 2. The wear progress shown in Table 3 (recorded at marked location in Fig. 10) confirms the measurement results regarding zero-film locations. After the tests with hardware configuration 1, the surface is in good condition. The instability with hardware configuration 2 led to abrasive wear beyond the outer sealing diameter. Moreover, initial wear can be observed at the outer diameter region due to increased moment M_t. The two deep scratches visible along the circumference of the running surface result from particles during operation. The wear profile after hardware configuration 3 confirms the measured thin film at the inner diameter region. The wear at the outer diameter region happens at 300 bar operating pressure due to elastic deformation of the valve plate at this position. Finally, the measured non-zero films in this study are in the same range as the films calculated for similar operating conditions with the help of the simulation model presented in [2]. The model itself was validated by measured leakage flows and valve plate temperature fields for several operating conditions.

5. CONCLUSIONS

The effect of two hardware parameters influencing the lubricating film thickness between cylinder block and valve plate could be confirmed by using ultrasound. The measured zero-film results are in agreement with the wear profiles taken of the valve plate, while the measured non-zero films match with the range predicted by simulation. The ultrasound method allows correlating the tested operating conditions without disassembly of the hydrostatic pump to the locations where thin-film conditions between valve plate and cylinder block with respect to hardware configuration take place. This is especially beneficial for finding the system limits. The ultrasound technique shows sufficient time resolution allowing the real-time observation of film thickness oscillations with shaft frequency and its higher orders. The findings will be utilized to support current product development activities and to validate and improve simulation models used for film thickness predictions [2].

6. REFERENCE

1. R.S. Dwyer-Joyce, P. Harper and B.W. Drinkwater, A method for the measurement of hydrodynamic oil films using ultrasonic reflection, in: Tribology Letters, Vol. 17, No. 2, 2004, pp. 337-348.
2. M. Zecchi, A novel fluid structure interaction and thermal model to predict the cylinder block / valve plate interface performance in swash plate type axial piston machines. PhD Thesis, Purdue University, ISBN-13: 978-0-615-98175-8, 2013.
3. J. Ivantysyn and M. Ivantysynova, Hydrostatic Pumps and Motors, 1st english ed., Akademia Books International, India, ISBN-81-85522-16-2, 2001.
4. J. Zhang, B. Drinkwater and R.S. Dwyer-Joyce, Calibration of ultrasonic lubricant-film thickness measurement technique, in: Measurement Science and Technology, Vol. 16, IOP Publishing Ltd, United Kingdom, 2005, pp 1784-1791.

7. AUTHOR CONTRIBUTIONS

L.L. designed the experiments. L.L. and P.H. prepared the hardware and carried out the experiments. S.M. processed the signals based on the procedure developed by P.H and R.D.J. Analysis and interpretation of the measurement results done by L.L. and S.M. Paper written by L.L. and S.M.